Electronic Supplementary Material (ESI) for Analyst.

Supplementary Information

For

Automated platform for cell selection and separation based on four-dimensional motility and matrix degradation

Hannah L. Nowotarski[a], Peter J. Attayek[b], and Nancy L. Allbritton[abc*]

[a] Department of Chemistry, University of North Carolina, Chapel Hill, North Carolina 27599, United States

[b] Department of Biomedical Engineering, University of North Carolina, Chapel Hill, North Carolina 27599, United States and North Carolina State University, Raleigh, North Carolina 27695 United States

[c] Department of Bioengineering, University of Washington, Seattle, Washington 98195 United States

[*]Corresponding author

Email: nlallbr@uw.edu

Microraft Segmentation. The bright field Z-stack was loaded into MATLAB to segment the microrafts and track microraft location at each time point (Fig. S1). A 3D Gaussian filter was applied to smooth the 3D reconstruction of the bright field stack and the mean intensity projection was subsequently calculated (Fig. S1A). The resulting 2D image was thresholded using Otsu's method (Fig. S1B).[14] Due to the curvature of the microraft borders, the borders appear much darker than the rest of the image and were easily segmented by Otsu's thresholding technique. Morphological operations were used on the binarized image to fill the area within the microraft borders. Any segmented objects that were smaller than 90% of a nominal microraft were removed, along with any microrafts touching the border of the image (Fig. S1C). For the initial time point, the MATLAB code identified the row and column of each segmented microraft within the image (Fig. S1D). For all subsequent time points, the segmented microrafts were registered to the initial time point segmentation using rigid transformation estimated by phase correlation.[15]

Cell Segmentation and Tracking. After the microraft segmentation, the fluorescence image stacks were loaded to segment individual cells on each microraft and track their centroid locations over the duration of the experiment (Fig. S2). Each fluorescence confocal stack was reconstructed in 3D and a 3D Gaussian filter was applied to smooth the reconstruction (Fig. S2A-B). For all times after the initial time point, the 3D reconstructions were transformed using the registration calculated from the bright field stacks. The 3D reconstructions were then binarized using a threshold set to 1.5 times the 90^{th} percentile of the voxel intensity values present in the reconstruction (Fig. S2C-D). All thresholded voxels outside of the segmented microraft area were removed so that only thresholded objects within the microraft borders remained. The resulting 3D binary image was then applied as a mask to the Gaussian smoothed 3D reconstruction of the fluorescence confocal stack and the local maxima of the masked 3D image were identified (Fig. S2E-F). The coordinates of local maxima that were closer than the minimum cell radius specified in the GUI were averaged together. Additionally, for all thresholded objects with multiple local maxima and a sphericity > 0.89, the coordinates of the local maxima within that thresholded object were averaged together to reduce over-segmentation of the cells. The sphericity cutoff enables the exclusion of oddly-shaped cells, such as those in mid-division. The resulting points were used as seeds for a seeded watershed algorithm to

identify individual cells (Fig. S2G-H).[16] The centroid of each segmented object was recorded for each time point along with the microraft that contained it.

In order to track individual cells between time points, a k-nearest neighbor search was used on the recorded centroids within each microraft at consecutive time points.[18] The results of the k-nearest neighbor search enabled the software to track cells from one time point to the next based on distance. The X, Y and Z distance each cell traveled over each time point was calculated. The GUI permitted a user to manually reject non-cell objects, cells that were dividing, or cells that were tracked incorrectly by the MATLAB software.

Collagen Image Analysis. Fluorescence image stacks of Alexa Fluor 488-labeled collagen on the microrafts arrays were used to determine collagen volume and thickness within the individual microrafts. First, the microrafts were segmented using bright field image stacks as described above. Next, the green fluorescence Z-stack was reconstructed in 3D and smoothed with a 3D Gaussian kernel. The 3D reconstructed image was then thresholded using Otsu's method. The percent of thresholded voxels were calculated above and within the boundary of each microraft.

Immunostaining Image Analysis. Fluorescence image stacks were acquired of cells labeled with Hoechst 33342 and immunostained with either an Alexa Fluor 594 or 647 secondary antibody. The cell nuclei stained with Hoechst were segmented in 3D as described above using the cell segmentation method. A morphological dilation was applied to the segmented nuclei using a spherical structuring element having a 25 μm radius to create a mask. The fluorescence intensity of the red fluorescence channel within the mask was integrated to determine the amount of immunostaining.

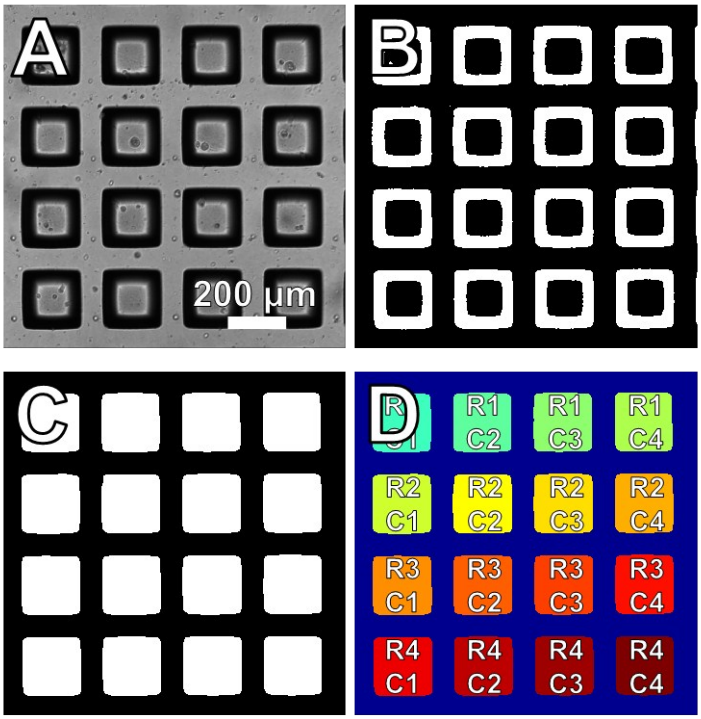

Fig. S1. Microraft segmentation and tracking. A) The mean intensity projection of the smoothed bright field image stack. B) The image was thresholded with Otsu's method. C) Morphological operations were used to fill holes, remove thresholded objects that were smaller than 90% of a nominal microraft, and remove any objects touching the image border. D) Segmented microrafts were labeled with row and column values.

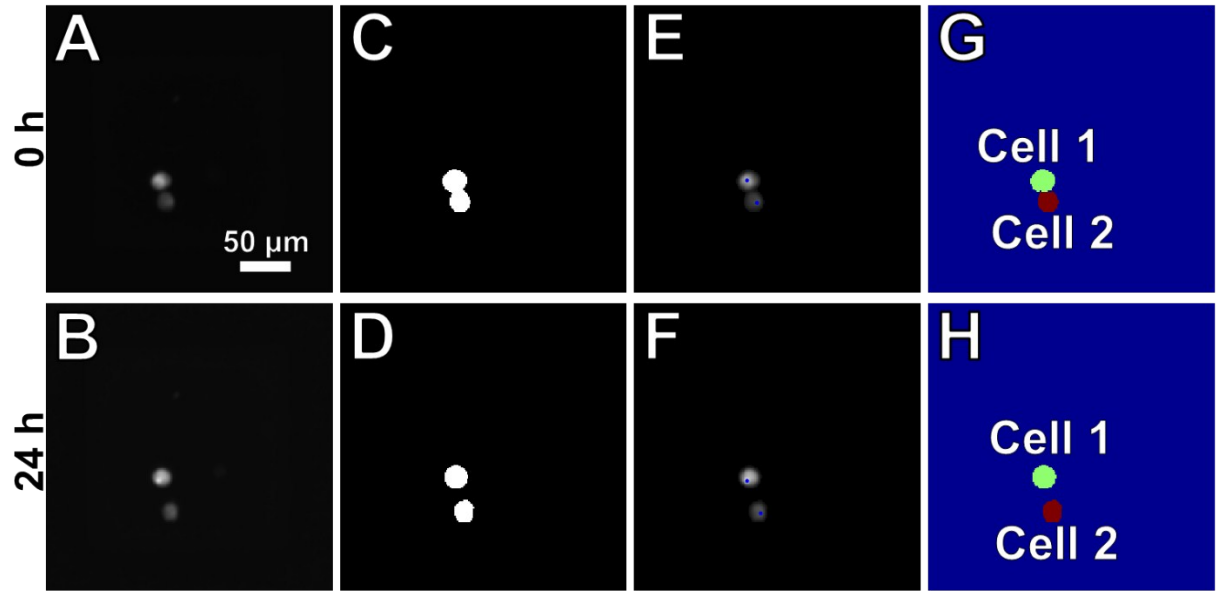

Fig. S2. Cell Segmentation. A-B) Max intensity projections of fluorescence confocal stacks that have been smoothed with a 3D Gaussian filter at 0 h and 24 h. C-D) The 3D confocal stacks were thresholded (2D projection shown). E-F) The local maxima within the thresholded voxels were identified (2D projection shown). G-H) A watershed algorithm was used to split touching cells and the individual cells were labeled.

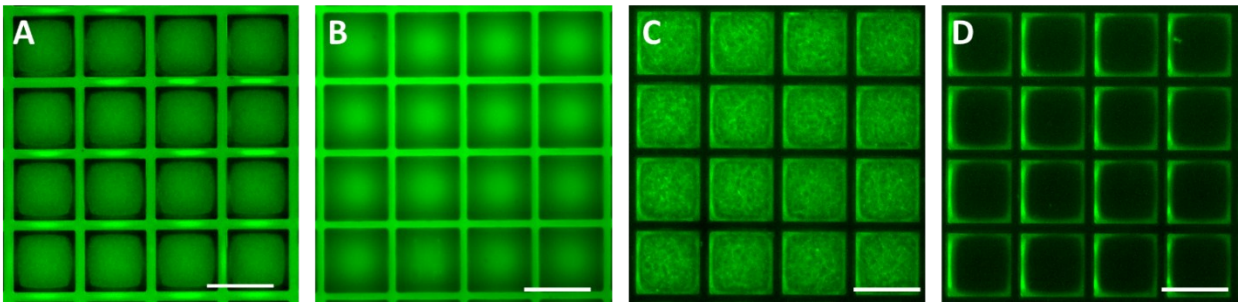

Fig. S3. Representative fluorescent images of A) fluorescein-conjugated Matrigel, B) Oregon Green 488-conjugated gelatin, and C) Alexa Fluor 488-conjugated collagen. D) Uncoated magnetic polystyrene microrafts. Scale bar is 200 μm.

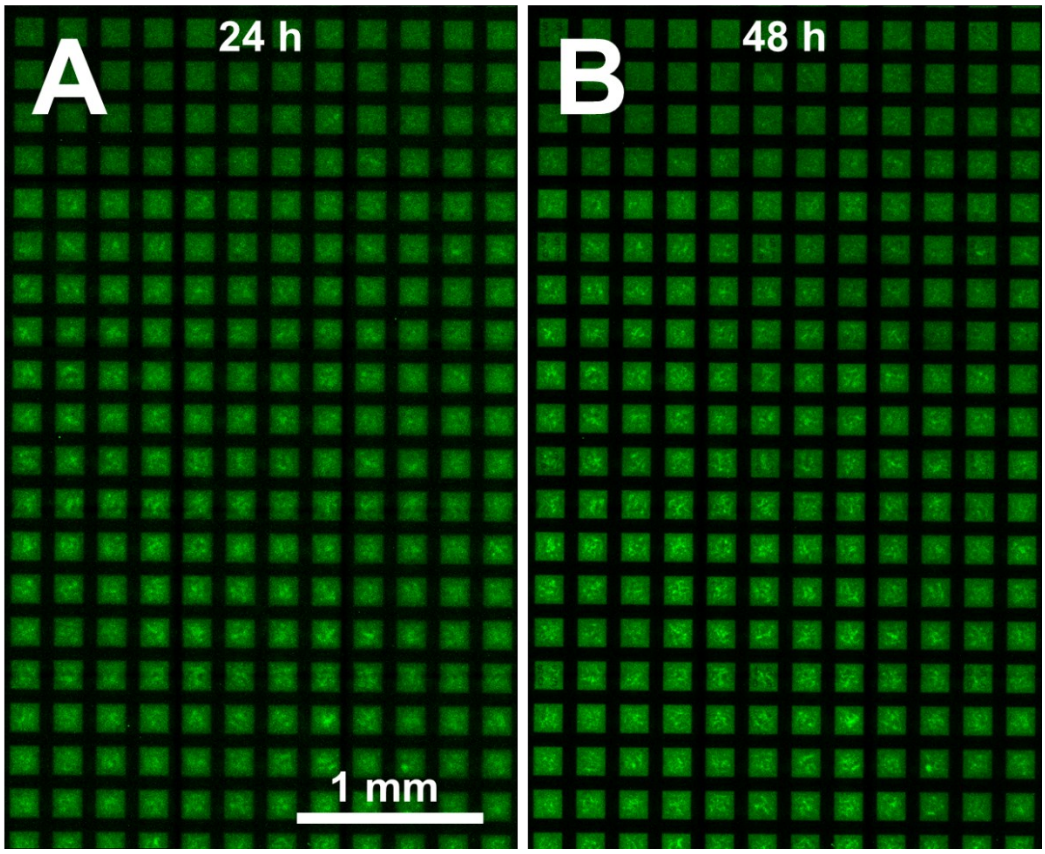

Fig. S4. Collagen stability in microwells over time. A) Large area scan showing fluorescein fluorescence of collagen in microwells after 24 h. B) Large area scan (same microrafts imaged as in A) showing fluorescein fluorescence of collagen in microwells after 48 h. There was no statistically significant difference ($p<<0.001$) between the mean fluorescein fluorescence per microwell normalized to the microraft autofluorescence at 24 h (1.22 ± 0.05 normalized RFU) and 48 h (1.31 ± 0.11 normalized RFU).

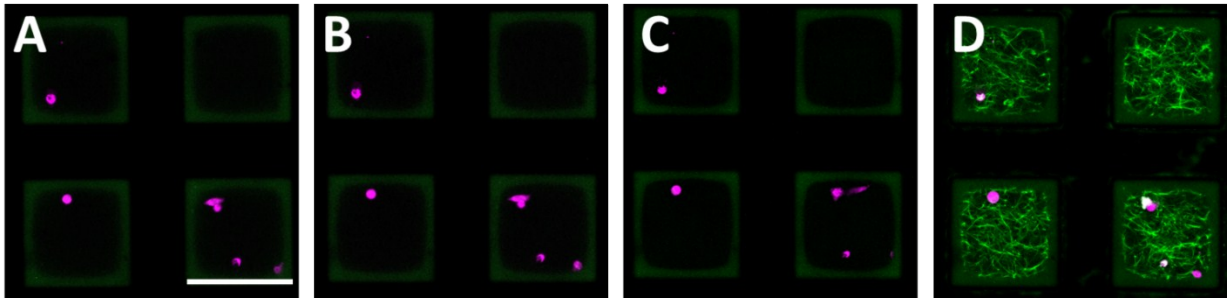

Fig. S5. Feasibility of cell entrapment in collagen. A) Maximum z-projection of red fluorescence of cells (pink) entrapped in un-stained collagen on a microraft array immediately after collagen polymerization. B) The same raft array region as in panel A after medium exchange. C) The same raft array region as in panel A after 24 h of culture. D) The same raft array region as panel A after 48 h of culture and after fluorescent conjugation of the collagen with Alexa Fluor 488Scale bar is 200 μm.

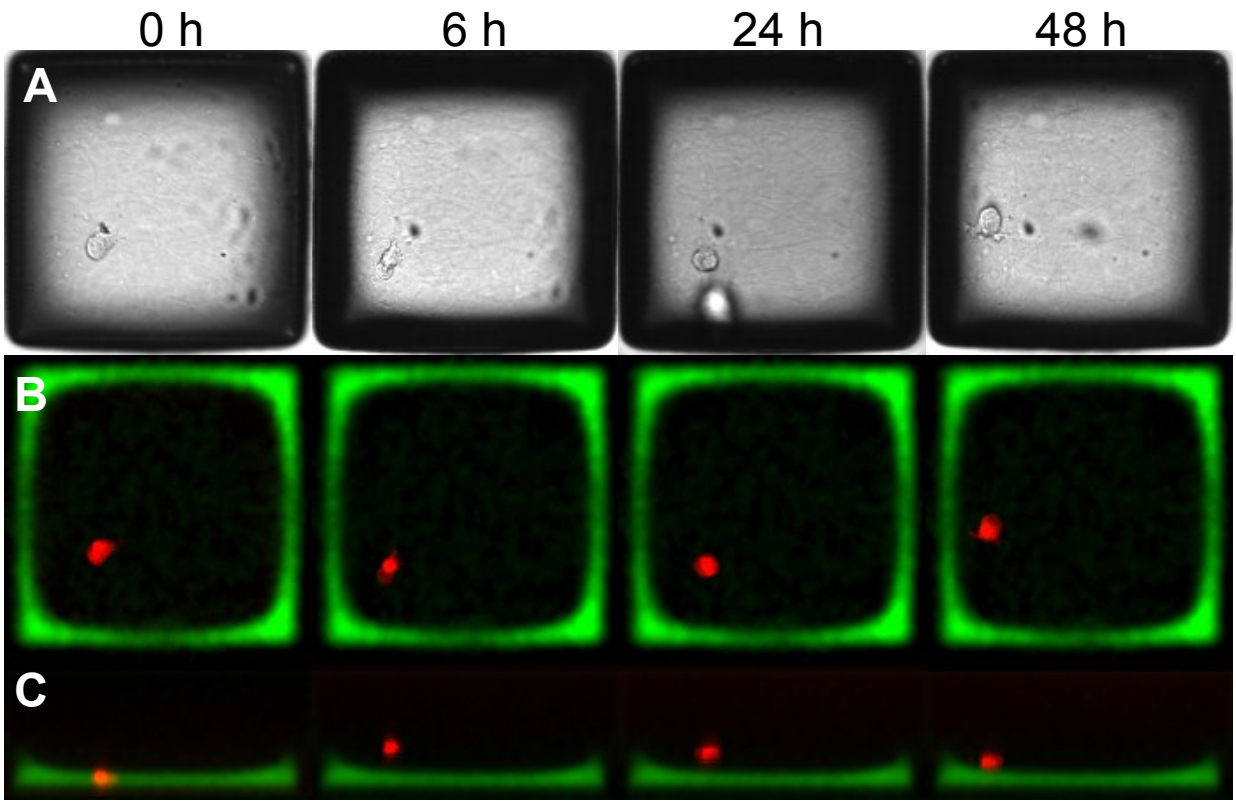

Fig. S6. Single cell tracking over time A) Brightfield image of a single cell embedded in collagen on a microraft over 4 timepoints. B) Composite fluorescent Z-projection of a single cell (red) in a microraft (green autofluorescence along the borders) over 4 time points. C) Composite fluorescent YZ-slice of a single cell (red) in a microraft (green autofluorescence) over 4 time points.

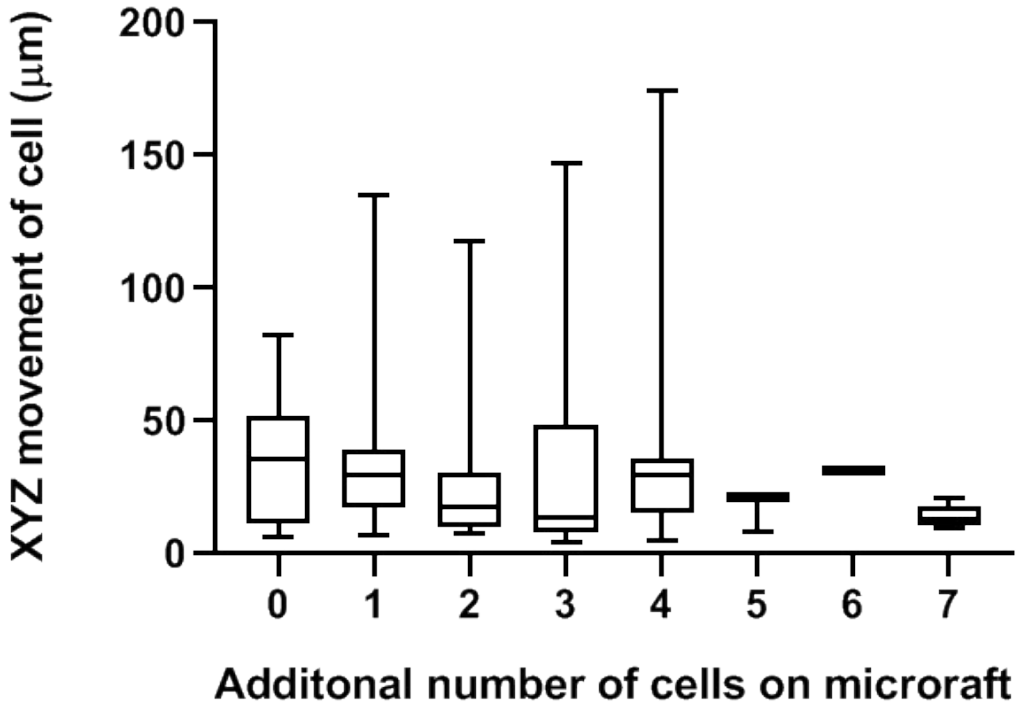

Fig. S7. Box and whisker plot showing XYZ movement between microrafts containing a single cell and those with multiple cells.

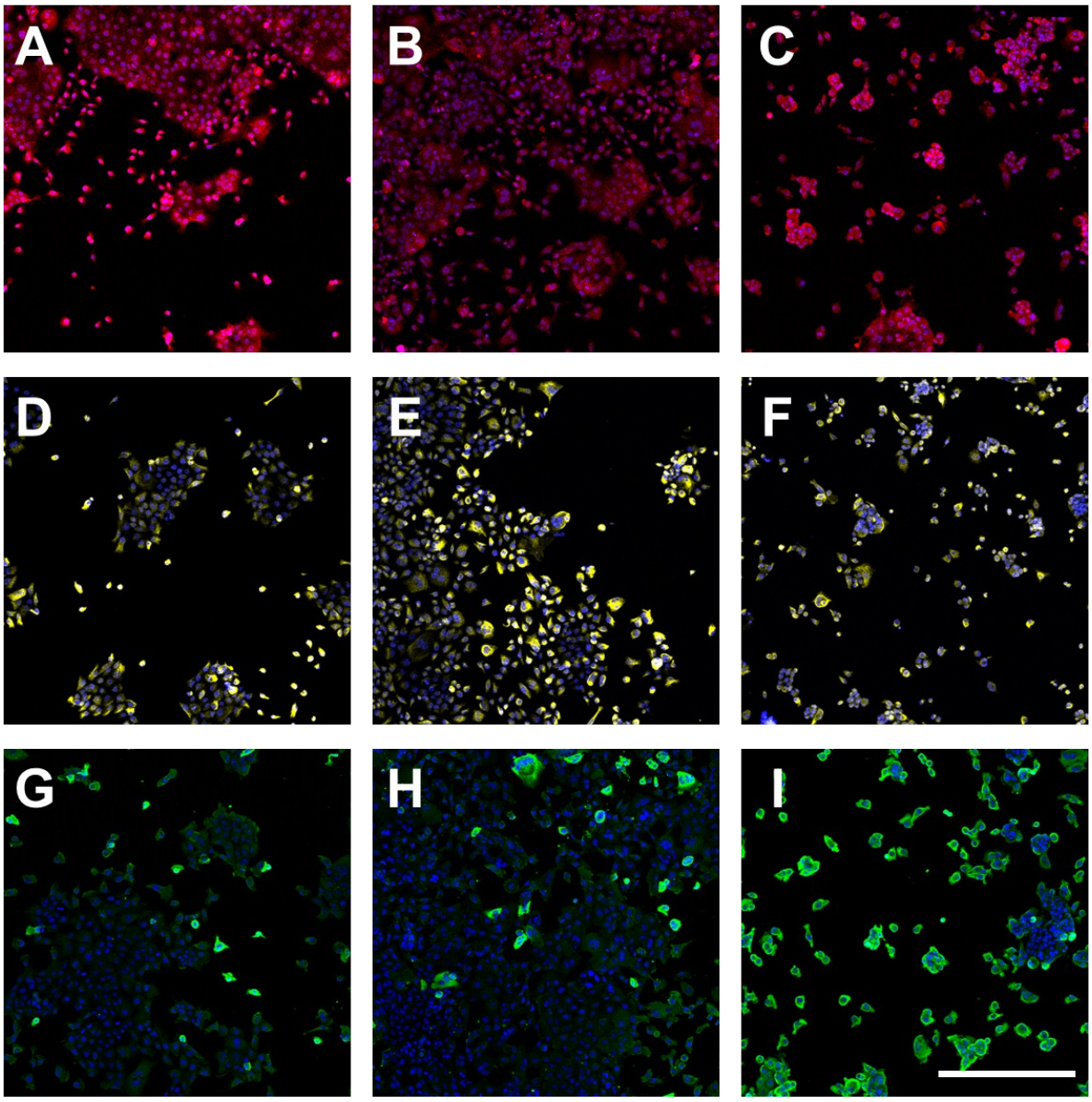

Fig. S8. Maximum z-projections of EMT fluorescence in CFPAC-1 populations A) Representative composite image of E-cadherin (red) and Hoechst 33342 (blue) fluorescence in bulk CFPAC-1 population. B) Composite image of E-cadherin (red) and Hoechst 33342 (blue) fluorescence in invasive CFPAC-1 population. C) Composite image of E-cadherin (red) and Hoechst 33342 (blue) fluorescence in non-invasive CFPAC-1 population. D) Composite image of vimentin (yellow) and Hoechst 33342 (blue) fluorescence in bulk CFPAC-1 population. E) Composite image of vimentin (yellow) and Hoechst 33342 (blue) fluorescence in invasive

CFPAC-1 population. F) Composite image of vimentin (yellow) and Hoechst 33342 (blue) fluorescence in non-invasive CFPAC-1 population. G) Composite image of α-smooth muscle actin (green) and Hoechst 33342 (blue) fluorescence in bulk CFPAC-1 population. H) Composite image of α-smooth muscle actin (green) and Hoechst 33342 (blue) fluorescence in invasive CFPAC-1 population. I) Composite image of α-smooth muscle actin (green) and Hoechst 33342 (blue) fluorescence in non-invasive CFPAC-1 population. Scale bar is 500 μm.